10
Near IR Spectroscopy for the Characterization of Dispersion in Polymer–Clay Nanocomposites

Q1
Q2 *Ana Vera Machado, J.M. Barbas, and J.A. Covas*

10.1
Introduction

Thermoplastic polymers reinforced with layered silicates can exhibit excellent physical and mechanical performance at filler contents typically lower than 5% in weight. Each individual clay sheet is hundreds to thousands of nanometers long and wide and has a thickness in the nanometer scale. Thus, its surface is quite substantial, of the order of hundreds of square meters per gram, yielding specific characteristics to the nanocomposite. However, as layered silicates are usually available as stacks of tactoids and their hydrophilic character is incompatible with the hydrophobic nature of polymers, dispersion into individual monolayers is difficult and has been the focus of intense research.

This chapter starts with a brief overview of the morphology and properties of polymer–clay nanocomposites, as well as of their preparation methods and characterization techniques. The use of near-infrared (NIR) spectroscopy for the characterization of dispersion in polymer nanocomposites is then discussed, with a focus on the application of inline techniques to monitor the preparation of polymer–clay nanocomposites by melt compounding.

10.2
Morphology and Properties

Simple mechanical mixing of a polymer with a silicate does not necessarily yield a nanocomposite. Depending on the interaction between polymer and clay surface, as well as on the thermomechanical environment created during mixing, separation of the clay stacks into discrete uniformly dispersed sheets may not be attainable [1–9]. Figure 10.1 shows a schematic representation of the possible polymer-clay composite morphologies resulting from mixing.

Immiscible composites are a consequence of the inability of the polymer to intercalate into the interlayer spacing (i.e., clay galleries). The clay remains in its agglomerate state, creating a micron-size dispersed phase. The properties of

Synthesis Techniques for Polymer Nanocomposites: Polymer Nano-, Micro- and Macrocomposites,
First Edition. Edited by Vikas Mittal.

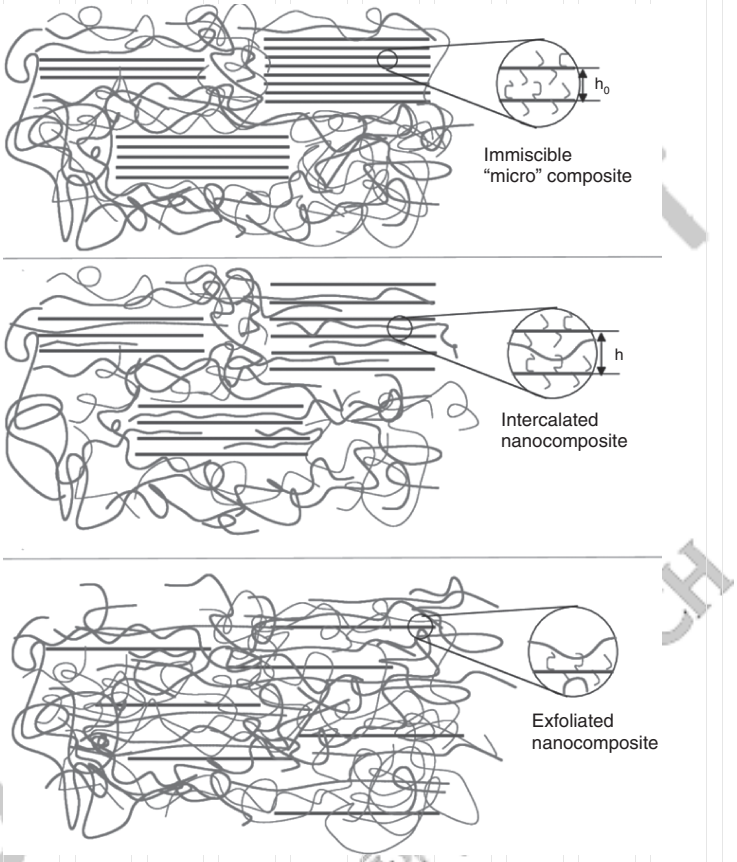

Figure 10.1 (a–c) Possible polymer–clay nanocomposite morphologies [9].

such materials are comparable to those of traditional microcomposites. The most beneficial morphologies are those maximizing polymer–clay interactions by producing a large interfacial area [9, 10]. They include intercalated and exfoliated systems. The term *intercalation* is associated with the polymer chains going in the interlayer, resulting in a multilayer ordered morphology. Intercalation increases interlayer spacing to approximately 2–4 nm [2, 3, 7]. Exfoliation corresponds to the complete delamination of all clay platelets. In this case, their separation exceeds 8–10 nm [2–4, 7]. In practice, most polymer–clay nanocomposites, particularly those prepared by melt mixing, have an intermediate morphology, comprising intercalated clay tactoids and exfoliated platelets [3, 7, 11–14].

High dispersion levels maximize polymer–clay interactions, enhancing mechanical properties, flame retardancy, and thermal stability, lowering permeability, and improving the catalytic effect on biodegradability of biodegradable polymers, while keeping optical transparency, low density, and processability [3, 8, 15–18].

10.3 Preparation Methods

Polymer–clay nanocomposites are obtained by intercalating polymer or monomer inside the galleries in between silicate layers, which will eventually lead to the delamination of individual platelets. The most important manufacturing routes are [2–4, 15–18] as follows:

1) *Solution intercalation* (*of polymer or prepolymer*) : This is a solvent-based method, in which the polymer solution replaces a suitable previously intercalated solvent. When using organic solvents, clay stacks can be easily dispersed. The polymer is adsorbed onto the layer surfaces, and on evaporation of the solvent the clay platelets return to equilibrium, fixing the polymer chains inside the galleries.
2) *In situ polymerization*: This was the first method used to prepare nylon 6-clay nanocomposites. It encompasses swelling of the modified clay by a liquid monomer or monomer solution, followed by polymerization triggered by heat or radiation, assisted by the diffusion of a proper initiator or catalyst that was previously fixed in the interlayer spacing by cationic exchange.
3) *Melt mixing*: In this case, clay and polymer are mixed in the molten state. Under the appropriate conditions, the polymer melt diffuses within the clay galleries, forming the nanocomposite. The process can be carried out in conventional polymer compounding equipment, representing a cost-effective and environmentally sound solution for the industrial scale production of polymer nanocomposites.

10.4 Characterization Techniques

Transmission Electron Microscopy (TEM) and X-ray diffraction (XRD) are the most commonly used techniques to characterize polymer–clay nanocomposites [2, 19–23]. TEM offers a direct observation of clay dispersion enabling, for example, to determine agglomerates/particle size and number of stacks/platelets per area. However, the technique analyzes only very small areas, requires time-consuming sample preparation, and quantification of morphology is tedious [2, 20, 21]. XRD presents a clear region of interest at low angles, because of the clay typical of Bragg's diffraction peak, from which the clay spacing and the stacks' height may be estimated. However, XRD fails to provide information on the spatial distribution of the clays within the matrix and is prone to interferences [2, 19–21]. Indeed, many factors, such as clay loading, orientation, and crystallinity, influence XRD intensity peaks. Efforts to develop a quantitative analysis of clay dispersion have combined TEM and XRD [22, 23]. The approach makes sense, as each technique is able to fill in the information gap of the other (see Figure 10.2, which shows TEM and XRD data for different stages of dispersion of a specific polymer–clay nanocomposite [20]). However, if the results are

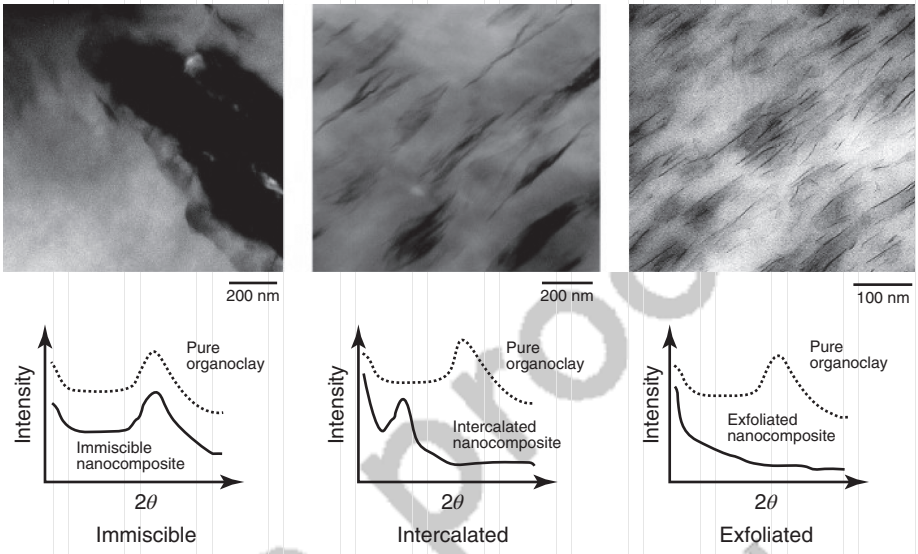

Figure 10.2 (a–c) Different states of clay dispersion, as observed by TEM and corresponding XRD spectra [20].

encouraging at local level, perceiving the overall state of clay dispersion of a given system would require an extremely time-consuming study [2, 20, 21].

As the rheological response of filled polymers is sensitive to structure, particle size, and shape, as well as interfacial characteristics, it is not surprising that it has been one of the most utilized tools for the characterization of nanocomposites [23–28]. Several authors have successfully related the rheological behavior with the state of dispersion [12, 14, 23, 25–30], while others used it to appraise distribution and structural effects [16, 23, 26–29]. The magnitude of the storage or loss moduli (G′ and G″) in the linear viscoelastic regime provides a good insight into dispersion quality, an increase of their values corresponding to finer dispersion [29], while the development of a plateau at low frequencies has been attributed to the deformation and recovery of dispersed particles [27–33]. Nevertheless, a quantitative analysis of filler dispersion based on rheological measurements is not frequently reported, as it is not easy to discriminate the effects of filler concentration and dispersion state on the rheological behavior [27, 31].

Recently, Lertwimolnun and Vergnes [12, 14, 29] proposed the use of a modified Carreau–Yasuda model with yield stress (σ_0) to describe the frequency dependence of the absolute complex viscosity:

$$|\eta^*(\omega)| = \frac{\sigma_0}{\omega} + \eta_0[1 + \lambda\omega^a]^{(b-1)/a} \tag{10.1}$$

where zero shear viscosity (η_0), relaxation time (λ), Yasuda parameter (a), and power law index (b) are adjustable parameters. As melt yield stress is generally associated with transition from liquid-like to solid-like behavior, in the case of clay nanocomposites it can be related to the formation of a percolated network

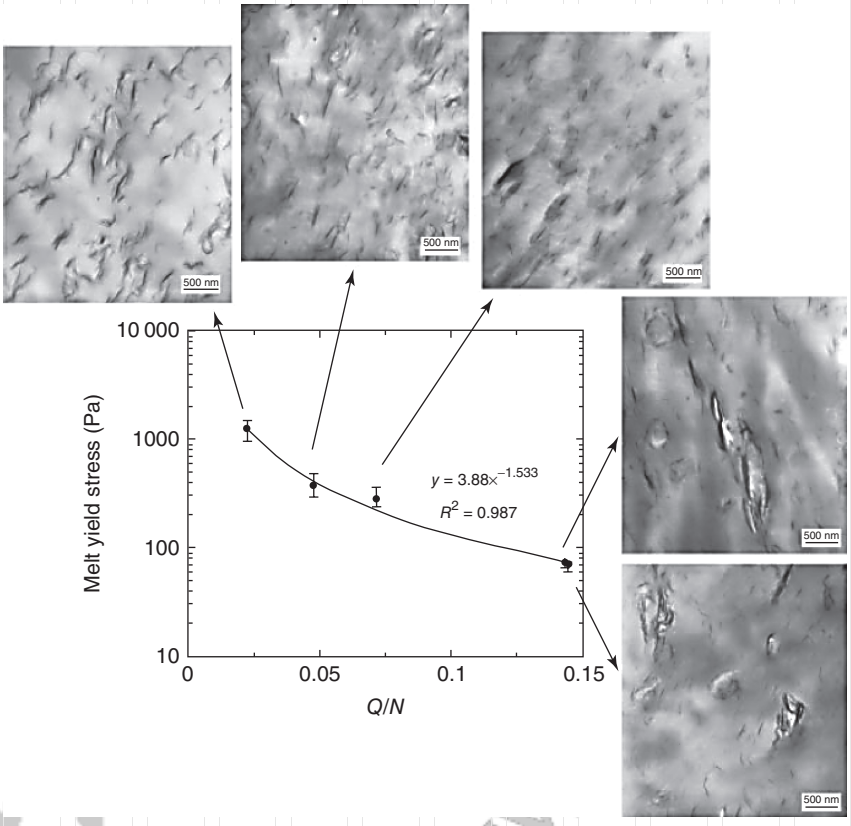

Figure 10.3 Evolution of melt yield stress as a function of filling ratio (output/screw speed, *Q*/*N*) for PP–clay nanocomposites prepared under different operating conditions [12].

structure of intercalated tactoids and exfoliated platelets [24, 28, 31–34]. As shown in Figure 10.3, Lertwimolnun and Vergnes correlated melt yield stress with the exfoliation of polypropylene (PP)-based nanocomposites prepared in a twin screw extruder and were able to quantitatively study the effects of operating parameters and material characteristics on dispersion. Alternatively, a power law expression for the complex viscosity (η^*) has been utilized for the low frequency range and related to clay dispersion [23–28]:

$$|\eta^*(\omega)| = K\omega^b \tag{10.2}$$

where power law index (b) and consistency (K) are adjustable parameters. Yet, the same dependence was found for high clay loading in a poorly dispersed composite and for good clay dispersion at lower clay concentration [23, 26].

Several spectroscopic techniques, such as nuclear magnetic resonance (NMR) and Fourier transformed infrared spectroscopy (FT-IR), have also been used to characterize morphology, surface chemistry, and dynamics of exfoliated polymer nanocomposites. VanderHart *et al.* [35–38] used solid state ^{1}H-NMR

to evaluate the degradation of the organic clay modifier through resonance positions. Also, considering the paramagnetic spin effects of the metallic cations present in the chemical composition of the clay, they utilized the relaxation spin times ($T_1{}^H$) measured by ^{13}C-NMR to evaluate clay dispersion. In principle, if the clay is poorly dispersed, the greater is the average distance between each polymer–clay interface and the weaker is the average paramagnetic contribution to $T_1{}^H$. According to some authors [4, 39–42], FT-IR is not only adequate to monitor clay dispersion, but is more efficient than XRD, as it can overcome the limit interlayer distance of 8 nm inherent to the latter, and less time consuming than TEM. In a FT-IR spectrum, the clay layers are easily differentiated from the polymer because of their Si-O bonds, causing a pronounced band between 1300 and 900 cm^{-1}. This band can be decomposed in at least four peaks, three of which are related to the Si-O in-plane vibrations (or bonds with basal oxygen) and one to the Si-O^- out-of-plane vibration (with apical oxygen or hydroxyl group). The former appear at about 1120, 1050, and 1020 cm^{-1}, whereas the out-of-plane vibration peak appears at about 1075 cm^{-1} [39, 41–44]. The area (or height) of the in-plane peaks ratio (1050 cm^{-1}/1020 cm^{-1}) increases with increasing interlayer spacing (intercalation), while the intensity of the peak at 1075 cm^{-1} rises with the spacing out of the individual clay layers (exfoliation). Also, when the morphology is ordered and intercalated, the original peak at 1050 cm^{-1} will display a negative shift toward lower wavenumbers, while that at 1075 cm^{-1} will shift toward higher wavenumbers for high intercalation or partial exfoliation [39, 40, 42]. Because of the trichroic clay behavior, preferential particle orientation may induce misleading conclusions in terms of intercalation/exfoliation levels. This can be overcome with the use of a polarizing lens [39, 42], which enables the measurement of spectra with different dipole moments. This is necessary for the subsequent calculation of the structural factor (SF) spectrum, which is equivalent to the spectrum with no preferential clay orientation.

Finally, tensile testing directly determines the reinforcing effect of the nanosilicate [2, 11, 15, 20], although the exact correlation with clay dispersion remains unclear. The reinforcing aptitude depends on several parameters, including the level of adhesion between filler and matrix, nanoparticle size and aspect ratio (individual layers, stacked layers, or tactoids), and nucleating role of the clays (which can significantly change matrix crystallinity). Early studies [45] showed a direct dependence of the reinforcing effect on clay dispersion, which was confirmed by others [7, 46] mainly for nanocomposites containing high polarity polymer matrices. For nonpolar matrices (like polyethylene or PP), incorporation of a maleated compatibilizer is often required to increase polymer-clay adhesion, thus maximizing the dispersion potential. However, it appears that beyond a critical concentration, the content of MA (maleic anhydride) is damaging, as the clay reinforcing effect is not able to exceed the reduced mechanical performance of the highly modified matrix. Bousmina [11] applied various shearing levels to the same polymer–clay system, obtaining nanocomposites with different dispersion states, as confirmed by TEM. Yet, as presented in Figure 10.4, the fully exfoliated sample

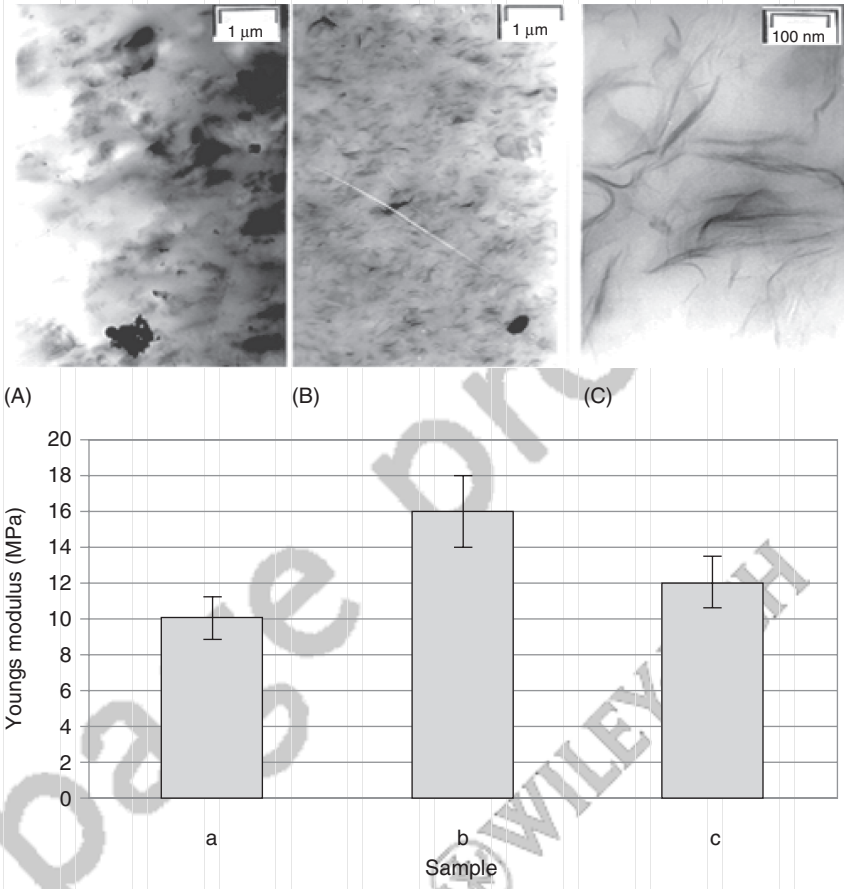

Figure 10.4 Polymer–clay nanocomposite showing different dispersion levels and respective Young's modulus [11].

exhibited an intermediate value of the Young's modulus. The author attributed this behavior to the flexibility of the individual clay sheets.

10.5 Dispersion in Melt Mixing

As Vaia *et al*. [47] demonstrated, polymer–clay nanocomposites can be obtained by direct melt intercalation, with attention concentrated on this route following its industrial relevance [6, 13, 47]. Proper dispersion is achieved when the intrinsic cohesive forces between clay layers are surpassed by the hydrodynamic stresses exerted by the polymer melt [3, 11]. Hence, extensive dispersion develops when four basic conditions are met: (i) an enthalpic driving force must exist for the polymer to penetrate the clay interlayer; (ii) the interlayer space should be at least

of the same order of magnitude of the diameter of the polymer macromolecular coil; (iii) sufficient residence time must be secured for diffusion; and (iv) a balance between stress and strain should occur, in order to attain a thermodynamically stable structure. During melt compounding, several parameters (screw speed, feed rate, set temperature, screw geometry) can influence these conditions, and consequently the resulting dispersion level [2, 3, 7, 11–15].

In recent years, the effects of matrix viscosity/molecular weight [48–50], chemical affinity of the polymer-clay interface [11, 31, 50–53], type of mixer and mixing protocol [7, 13, 54, 55], and operating conditions (screw speed (N) and throughput (Q)) have been investigated [7, 12, 14, 29]. For example, for a polypropylene/polypropylene grafted with maleic anhydride/Cloisite 20A (PP/PP-g-MA/C20A) system, Lertwimolnun and Vergnes [12] concluded that higher exfoliation is achieved with low Q/N ratios, that is, higher screw speeds and lower feed rates (Figure 10.3). It is well accepted that the dispersion mechanism of organoclays combines the diffusion of the polymer chains within the clay galleries (intercalation) and the exertion of sufficient mechanical forces to delaminate the individual platelets (exfoliation). Generally [7, 11, 54]:

- Intercalation is nearly independent of processing conditions, but sufficient residence time is critical to enable polymer melt diffusion inside the layer spacing;
- Exfoliation is extremely dependent on the chemistry, as well as on the mechanics and physics of the melt mixing process;
- A balance between time for diffusion and deformation (shear or extensional) for exfoliation is required;
- If melt mixing conditions favor high polymer chain mobility and if proper chemical affinity exists, exfoliation can develop even at low shear rates.

Dennis *et al*. [7] proposed a dispersion mechanism that includes a diffusion-controlled route during which shear-controlled fracture of the organoclay particles takes place, along with the sequential intercalation of the polymer, or the peeling of the individual clay layers from the top and bottom ends of each clay stack [3, 7]. The first pathway is chemistry dependent: if the compatibility between clay surface and matrix is high, well-exfoliated nanocomposites can be prepared for virtually any set of processing conditions [7]. This hypothesis has been proposed in most studies of polyamide-based nanocomposites [17, 18, 20, 25, 30, 38, 56, 57]. The second route is valid for marginally compatible polymer–clay systems, which is the case of most polyolefin-based systems [12, 14, 19, 29, 52, 54]. Under these circumstances, both chemical affinity and processing conditions should be optimized in order to attain enhanced clay dispersion. The third route presumes no compatibility between clay and matrix. Although processing conditions can be adjusted, it will be difficult to reach a nanoscale dispersed phase. Increasing shear should lead to improved dispersion through sliding of adjacent platelets (this requires high shear intensity), followed by diffusion of the polymer chains into the clay galleries and partial peeling of the platelets, starting from the edges. More recently, Bousmina [11] showed that the diffusion of polymeric chains inside the clay galleries is improved under

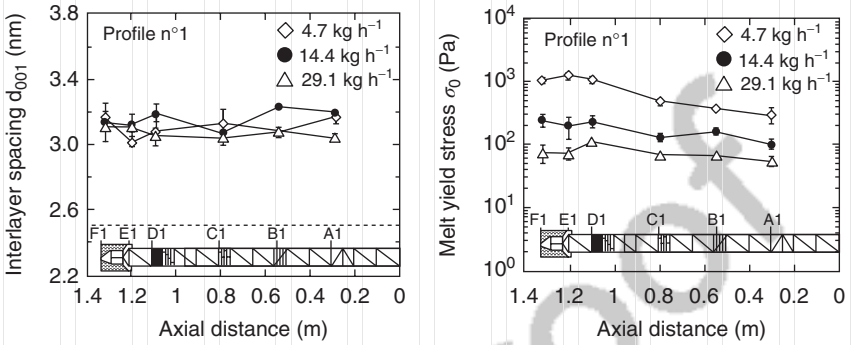

Figure 10.5 Effect of feed rate on the variation along the extruder of interlayer spacing (a) and melt yield stress (b) [14].

mild shearing conditions (or in a medium to low viscosity matrix) applied during sufficient time, whereas extensive exfoliation requires a high level of shearing/deformation.

Most of the above studies involved small-scale experiments [11, 49, 52] and/or the characterization of samples collected after completing mixing [29], for example, at the extrusion die exit [7, 13]. The evolution of clay dispersion along an extruder, where a complex nonisothermal 3D flow develops, seems to be less well understood. Lertwimolnun and Vergnes [12, 14] characterized postmortem samples collected from various locations along the axis of a corotating twin screw extruder (TSE). They concluded that both intercalation and exfoliation can reach relatively high levels immediately after melting. They also observed that less restrictive screw profiles yielded better dispersion levels. Furthermore, depending on the combination of screw profile and operating conditions, these authors observed an apparent reversion of dispersion evolution along the screw. This is illustrated in Figure 10.5 for the effect of feed rate. The graph on the left presents the evolution of the interlayer spacing (d_{001}), as determined by XRD, which is associated with intercalation. The plot on the right presents the progress of melt yield stress, which is linked to exfoliation.

10.6 Online and Inline Monitoring of Dispersion

During practical compounding and processing, the parameters that are continuously monitored (typically temperature, melt pressure, and motor torque) do not provide sufficient information on the characteristics of the system being processed. Thus, the possibility of assessing in real time the dispersion of a nanocomposite on processing is an important scientific and technological target, as it can be used to assist the definition of material recipes, the optimization of operating conditions and/or screw design, as well as for quality control and, ultimately, process control.

Implementing several of the characterization techniques discussed above as process monitoring tools seems a difficult and expensive task. XRD is feasible [58], but entails substantial modifications of the processing equipment and, eventually, the use of synchrotron radiation [59–65]. Rheology has been a more viable alternative, with academic teams [66–72] and rheometer manufacturers [56, 57, 73, 74] attempting to develop reliable, precise, simple to operate, and economically attractive inline and online equipments. Inline fixtures are preferred, as they avoid melt bypasses [66, 68–71, 75], but are obviously more difficult to design. Generally, they consist of modified dies. Most commercial solutions use capillary or slit rheometers to provide online measurements [56, 73, 74] between extruder and die and involve the continuous deviation of the melt from the main flow to the rheometer, as set by means of a gear pump. Online solutions seem easier to adapt to the different processing equipments and, at least conceptually, could also be fixed upstream, along the barrel of the extruder. Then, it would become possible to monitor the evolution of dispersion along the extruder axis. In this regard, the Piezo Axial Vibrator is interesting, as its feed port has the standard geometry of a melt pressure transducer [57]. Generally, online devices should (i) minimize the time lag between sample collection and measurement; (ii) prevent material morphology changes both during sampling and measurement; (iii) enable measurements along the axis of the extruder; and (iv) be capable of performing measurements at temperatures different from the processing temperature.

Taking advantage of the modular construction of most corotating TSEs, Covas *et al.* [67] developed an online capillary rheometer that can be fixed at different axial locations and is capable of quickly collecting material samples from within the extruder. The device was successfully used to study the viscosity evolution along the screw of various polymer systems, thus contributing to better understand the corresponding mixing and/or chemical mechanisms. Later, an online rotational rheometer, capable of working either in steady shear or oscillatory mode, was built [72]. The authors measured the evolution of the rheological moduli (G' and G'') of a noncompatibilized and equivalent compatibilized polymer blend. It was shown that the use of online rheometry reduces the effects of degradation and morphology alterations that can take place during sample collection and subsequent preparation for offline characterization, because of the successive thermal cycles that the samples are subjected to. An improved automated version of the prototype was applied to the rheological characterization of a polypropylene/polypropylene grafted with maleic anhydride/Dellite 67G (PP/PP-g-MA/D67G) nanocomposite along the axis of an extruder [76]. The G' and G'' curves depicted in Figure 10.6, obtained in small amplitude oscillatory shear (SAOS) at three different axial locations (3, 5, and 7, in the downstream direction) clearly show a plateau at low frequencies and an increase of the moduli values, that is, of dispersion, as the material progresses along the screws.

Several spectroscopic techniques have also been efficiently applied to online/inline process monitoring [77–80]. These include Raman [81–85], ultra violet-visible (UV-Vis), fluorescence [83–86], and attenuated total reflectance

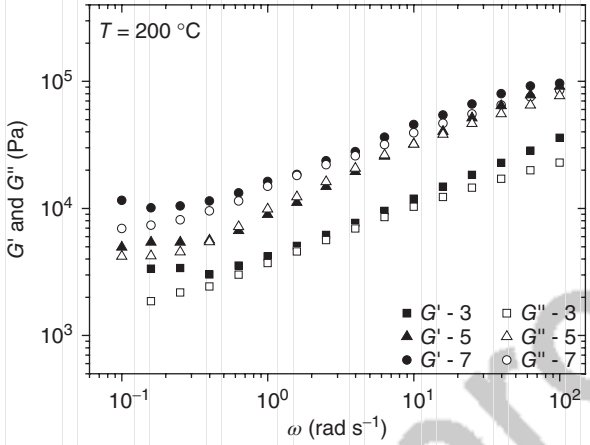

Figure 10.6 Linear viscoelastic behavior of PP/PP-g-MA/D67G nanocomposite at 200 °C, measured online at three axial locations (3, 5, and 7, in the downstream direction) along a corotating twin screw extruder [76].

medium infrared (ATR-IR) [81, 82, 87, 88], ultrasound (US), dielectric probing [77, 81, 89–91], and NIR spectroscopy [79–81, 92, 93]. Inline monitoring in polymer processing using NIR is performed mostly in transmission mode, using a flow-cell fixture attached to a modified extrusion die [79, 81, 83–85, 94–97], or to the nozzle of an injection molding machine [93, 98]. The polymer industry has a tradition of using NIR to monitor polymerization, copolymerization, and depolymerization reactions [96, 97, 99–104], particle size control [96, 105, 106], and other polymer-related operations [79, 81, 84, 93, 95, 99]. NIR is also commonly used to characterize clay minerals, to study their chemical modification, adsorption mechanisms [107–110], and structure [111, 112]. In the polymer nanocomposites field, NIR has been utilized to study the reinforcement effect of the clay [113] and to monitor melt processing [78, 98, 114]. In the first case, NIR spectra measured offline showed a direct correlation with the reinforcement effect determined by melt extensional measurements. Moghaddam *et al*. [98] used NIR to follow the preparation of thermoplastic polyurethane (TPU) nanocomposites in a small-scale extruder. A decrease of typical urethane bonds during processing was detected and attributed to the softening of hard segments during the initial 4–6 min and to the degradation of TPU [98]. Witschnigg *et al*. [114] fixed an NIR probe between extruder and die to study the effect of screw speed and screw geometry on the properties of polymer–clay nanocomposites. Single parameter chemometric models based on Young's modulus, interlayer distance, and drawing force were developed, good correlations with measured values having been obtained in some cases. However, confidence on the calibration lines seemed insufficient to perform a quantitative analysis. Recently, Fischer *et al*. [78] coupled NIR, US, and Raman probes to a bypass adapter fixed between extruder and die to monitor the preparation of nylon-6 nanocomposites with several organoclays. The correlation between NIR spectra and level of dispersion was based on a single

parameter chemometric model, using the shear thinning power law index, as proposed by Wagener *et al*. [25], good results having apparently been obtained.

Because of the complexity of NIR spectra, adequate chemometrics seems essential to extract from the data as much relevant information as possible. Chemometrics is a step-by-step methodology aiming to develop a calibration model relating the NIR spectral data with the reference characterization parameters [115–118]. To guarantee effective predicting capabilities, it must encompass model development and validation [117, 119]. The multivariate calibration technique uses the entire spectral structures, instead of a single spectral data point, to offer broader information, and thus detect even minute differences in the sample spectra [116, 119]. During model development, a predefined group of samples (usually designated as "training samples") is used to compute the calibration curve, which directly yields the analyte property from the respective spectra. To ensure precision, the degree of correlation between spectral and reference data should be high. For this purpose, a cross-validation step attests the quality of the adjustment of the data points to the calibration curve. More specifically, a certain number of the training samples are selected and the predicted property is compared with the reference values [116, 119]. Finally, the calibration model can be used to predict the characteristics of unknown samples. Therefore, chemometrics represents both NIR major advantage and limitation, as an adequate chemometric analysis may require extensive experimental characterization and data treatment, as well as the development of multiparameter calibration models [115–119].

The authors used a commercial NIR setup and a comprehensive calibration model to monitor clay dispersion in a polymer matrix, both in terms of evolution in time and final level attained, in a Haake batch mixer and in a corotating TSE. The system comprises three main components (Figure 10.7): (i) a diffuse reflectance probe (Axiom Analytical Inc.) with a sapphire window having a diameter of 5.7 mm; (ii) a Matrix® F (Bruker Optics) spectrophotometer; and (iii) the OPUS® Quant2 (Bruker Optics) data acquisition and analysis software. The probe communicates with the spectrometer via a fiber optics cable and the spectrometer connects to the workstation by a LAN-type cable. In the case of the Haake mixer [120], a threaded hole with Dynisco-type geometry was machined in the front plate of the mixing chamber to accommodate the NIR probe. The NIR spectra were measured with a resolution of 8 cm^{-1} and accumulation of four scans, the acquisition time for each spectrum being less than 2 s. During the initial mixing stages, because of the melting of the matrix and the presence of large voids, the spectra were generally very noisy and had very low absorbance. Consequently, for chemometric purposes acquisition started once the onset of equilibrium torque was reached (this occurred typically after 2 min of mixing). Thus, it was possible to collect 150 spectra during each mixing cycle.

Q6 Preparation of a Polypropylene/Polypropylene grafted with Maleic Anhydride/Montmorillonite/Cloisite 20A system (PP/PP-g-MA/C20A), using different PP-g-MA contents and operating conditions, was adopted as a case study [120]. To develop a calibration model, the usefulness of parameters derived from well-established characterization techniques, able to discriminate between

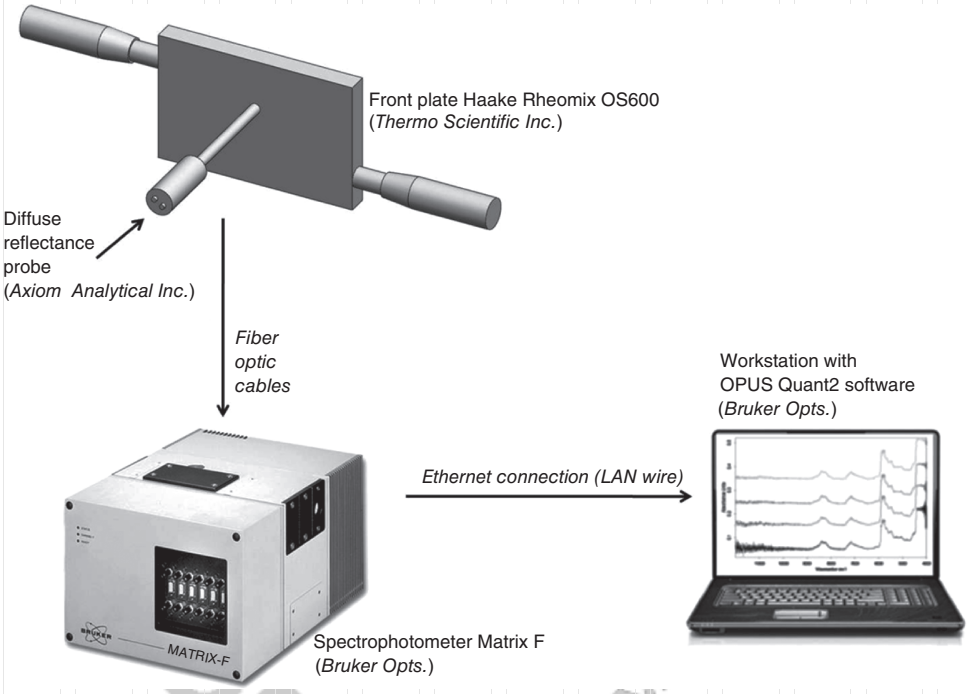

Figure 10.7 Inline NIR setup and coupling to the Haake mixer.

distinct dispersion levels, was initially evaluated. Single parameter calibration models from XRD, rheology, FT-IR, tensile testing, or torque data were globally inadequate. Multiparameter models showed greater potential, particularly when incorporating sufficiently performing individual building blocks. Specifically, a 7-parameter model combining parameters from oscillatory rheometry (G', G'', σ_0, b), FT-IR (wavenumber shift of the peaks at 1050 and 1080 cm^{-1}), and thermomechanical data from the mixing equipment (maximum torque) yielded good results. When applying it to real-time monitoring of the evolution of dispersion on the mixing of the same system under distinct operating conditions, or of the nanocomposite containing different levels of compatibilizer, not only coherent results were obtained, but they also matched well the forecasted values. As an example, Figure 10.8 presents the evolution in time of torque and predicted dispersion level for two case studies. The initial spectrum (at 0 s) is close to zero. As mixing evolves, both the baseline and the signal intensity increase. As seen in the torque curve, melting starts after around 10–20 s of mixing. The increase in torque is because of the conversion of a granular flow into that of a melt suspension with high solids content. Although the NIR signal is weak, the fundamental peaks are already visible and clay dispersion is predicted to be initiated. The torque reaches its maximum at about 30 s and decreases thereafter, as melting progresses. Melting is probably completed at around 90–120 s, but it is only after mixing for 180 s that a torque plateau is reached, which most

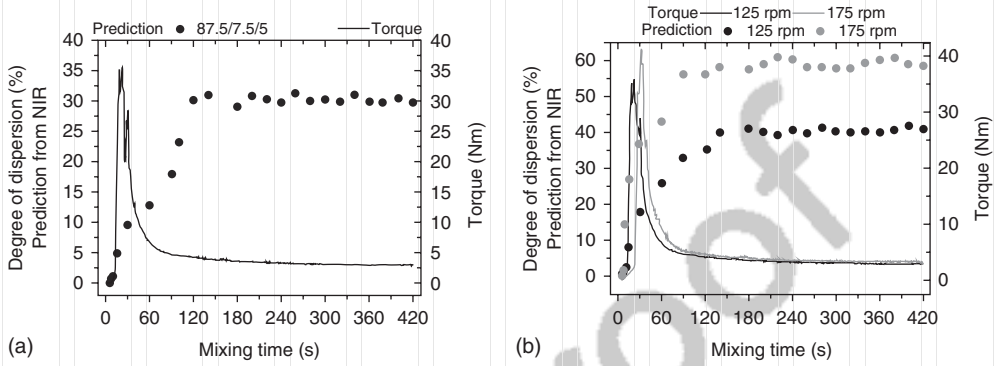

Figure 10.8 Evolution of torque and (predicted) average dispersion with mixing time during the preparation of a PP/PP-g-MA/Closite 20A nanocomposite in a Haake mixer: (a) 87.5/7.5/5 w/w% at 50 rpm and (b) 90/5/5% at 125 and 175 rpm.

likely corresponds to little further changes in dispersion. In fact, it has been recurrently reported for several systems melt mixed in batch mixers or twin screw extruders that most of the dispersive mixing takes place on melting, when the thermomechanical stresses are higher and little evolution being detected thereafter [121, 122]. Differences in the NIR spectra up to 180 s are also high, whereas after that period the spectra are almost superimposed. Thus, the rate of dispersion is predicted to be higher between 60 and 150 s, a plateau being foreseen thereafter. The predicted final dispersion level (after 180 s) for the sample with 7.5 wt% of PP-g-MA is roughly 30%, which connects well with the normalized average values of the samples with 5% and 10 wt% of PP-g-MA, 26.3 and 36.9%, respectively. It is also in agreement with reports relating the improvement of clay dispersion in polyolefin matrices with the increase in compatibilizer content [29, 53, 123]. In the case of the 90/5/5 w/w/w nanocomposite, the final dispersion level is predicted to increase with rotor speed (approximately 39 and 59% at 125 and 175 rpm, respectively). Again, these values are in line with the normalized averages (23.5%, 49.6%, 77.2% for 100, 150, and 200 rpm, respectively) and with reports showing an increase in dispersion with increasing rotor speed [29, 53].

The study above was performed using a diffuse reflectance probe, as the adoption of a probe operating in transmission would imply flow of the material out of the batch mixer. However, it is important to verify if operation in reflectance mode is adequate for practical inline monitoring during extrusion. This was done for a Polypropylene/Polypropylene grafted with Maleic Anhydride/Organo-Montmorillonite (PP/PP-g-MA/D67G) system prepared in Leistritz LSM30.34 twin screw extruder [124]. Figure 10.9 shows the spectra in the two modes for a 90/5/5 wt% composition, prepared under different screw speeds. They are similar in the region 9000 – 5000 cm^{-1}, although signal variations in transmission are more pronounced. In the lower wavenumber region (6000 to 4500 cm^{-1}) the reflection spectra have worse definition, while the transmission signal shows some saturation (absorbance above 2.0). Although chemometric models should

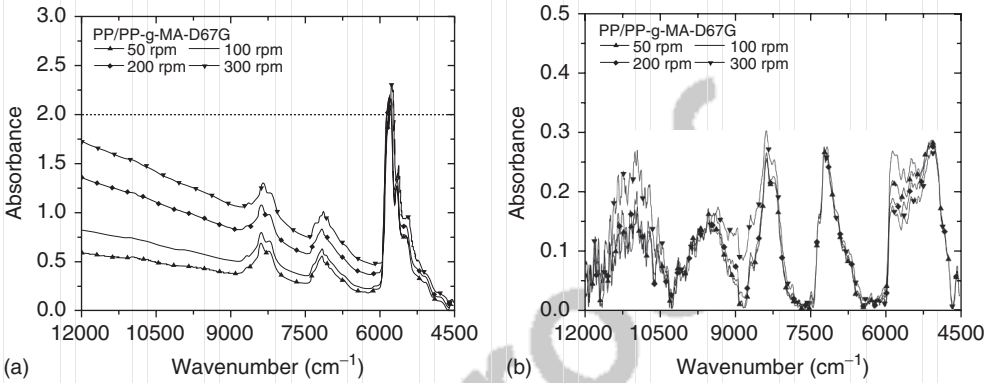

Figure 10.9 NIR spectra of the PP/PP-g-MA/D67G 90/5/5 wt% nanocomposite prepared under different screw speeds: (a) Transmission and (b) Diffuse reflectance.

not be extended to materials or processing conditions outside the range utilized to create them [123], the same model was used here [120], as one would anticipate that throughput and screw speed are variables influencing the same dispersion mechanism.

Table 10.1 ranks the predicted relative degree of dispersion of the samples. Dispersion should not increase strictly with output, a maximum being anticipated at intermediate throughputs. Similar to the effect of screw speed, this behavior could be because of the conflicting effects of higher hydrodynamic stresses and lower residence times with increasing feed rate. Nevertheless, other factors may also come into play, as the higher shear rates associated with the higher outputs boost viscous dissipation and this may trigger polymer degradation. In turn, the degraded material will become less viscous and could outflow from between the clay platelets, thus delaying or even reducing dispersion. At the same location of the inline measurement, samples were collected from the extruder and characterized offline.

The evolution of clay dispersion along the axis of the same TSE was investigated for a PP/PP-g-MA/D67G system [125, 126], utilizing the diffuse reflectance probe (see setup in Figure 10.7) fixed at various axial barrel locations and contacting directly the melt stream. Using the same chemometric model [120], the predictions along the extruder are presented in Figure 10.10. The evolution is consistent with the rheological measurements (not shown). For the three screw

Table 10.1 Average dispersion level of PP/PP-g-MA/D67G 90/5/5 wt% nanocomposites prepared under various throughputs.

	Relative degree of dispersion (± error) (%)			
Q (kg h^{-1})	1.5	3	6	9
NIR prediction	32.0 (± 1.7)	51.6 (± 1.1)	73.0 (± 3.5)	35.4 (± 4.2)
Normalized average	30.1 (± 3.8)	51.0 (± 3.2)	70.1 (± 3.8)	40.4 (± 4.0)

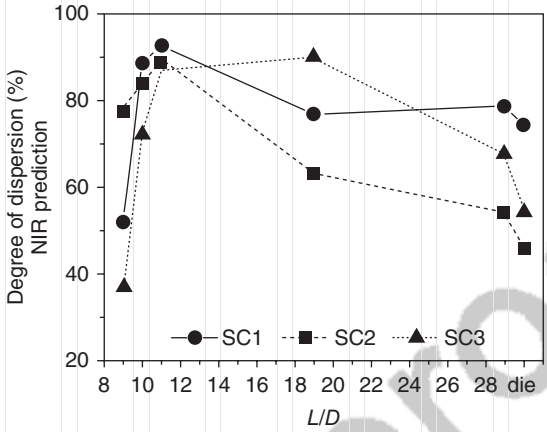

Figure 10.10 Inline NIR real-time predictions of the evolution along the screw axis of the average clay dispersion in a PP/PP-g-MA/D67G system, when using three different screw profiles (coded SC1, SC2, and SC3).

profiles tested (SC1, SC2, and SC3), dispersion evolves fast along the first mixing zone ($L/D = 9–11$) and then beyond $L/D = 11$ it either remains roughly constant or regresses. Reversibility is more significant for SC2.

Figure 10.11 displays the effect of screw speed, as determined by inline NIR and rheometry (melt yield stress, σ_0). Inline NIR measurements started at $L/D = 10$, when melting appeared mostly completed. As seen in Figure 10.11a, at $L/D = 10$ dispersion levels are already significant (between 37 and 89%, depending on screw speed) and increase sharply until $L/D = 11$ (values between 70 and 93%). Thus, dispersion evolved rather quickly, simultaneously with completion of matrix melting, because of the high stresses and deformations generated by the restrictive screw elements and the local lower material temperatures. This behavior resembles the evolution of morphology and chemical conversion during *in situ* compatibilization of polymer blends, with high developing rates on melting [14]. From $L/D = 11$ onward, a plateau or a decrease in dispersion is predicted, the latter being especially perceptible in the die. Rheological measurements (Figure 10.11b) were performed from $L/D = 11$ onward (in this case, it is essential assure a fully molten matrix), and show the same trend, that is, a constant or lower dispersion along the second part of the extruder and die (except for the composite prepared at 50 rpm). At $L/D = 11$, melt yield stress increases with screw speed, that is, exfoliation is promoted. Figure 10.11c,d depicts the data of Figure 10.11a,b, respectively, but normalized to the values measured at $L/D = 11$. Both indicate that (i) the rate of dispersion evolution along the screw decreases with increasing shear rate, that is, at low screw speed, dispersion progresses axially, at intermediate speeds, little changes take place, at high screw speed, reversion apparently occurs and (ii) flow along the die has a negative impact on dispersion. This result was globally confirmed by other dispersion assessment techniques, like X-ray and TEM. Reversion of dispersion with increasing screw speed seems to be induced by the parallel

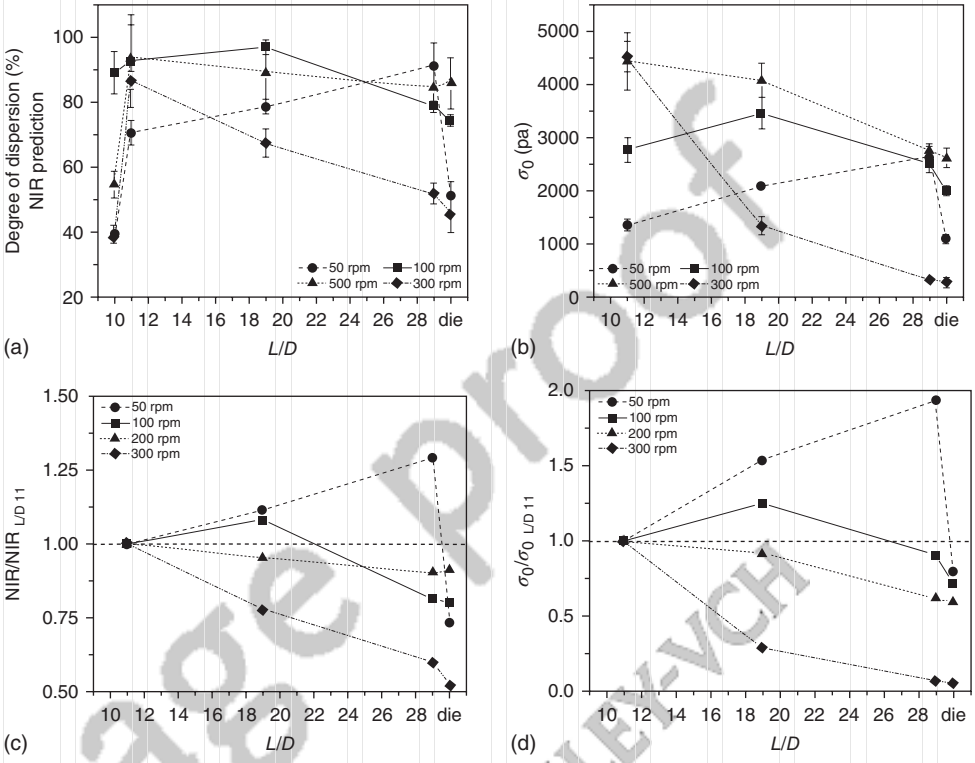

Figure 10.11 Effect of screw speed on the evolution of dispersion of a PP/PP-g-MA/D67G nanocomposite along the extruder axis, as determined by: (a) inline NIR; (b) rheology (melt yield stress); (c) same data as (a), but normalized to the values measured at $L/D = 11$; and (d) same data as (b), but normalized to the values measured at $L/D = 11$.

increase of viscous dissipation and degradation of the clay surfactant. The latter reduces clay-polymer affinity and, together with the decrease in melt viscosity affected by viscous dissipation, enables diffusion of the polymer chains out of the clay galleries. Degradation of the clay surfactant could also induce degradation of the polymer matrix by chain scission, with a further decrease in viscosity. Reversion of dispersion with increasing feed rate was related to relaxation phenomena.

The evolution of dispersion of a polyamide 6-clay nanocomposite and the effect of operating conditions were also assessed by NIR [127]. The experimental procedure followed was identical to that for the PP system discussed above. Figure 10.12 displays the influence of screw speed and output on final clay dispersion, as determined by XRD, rheology, and inline NIR (Figures 10.12a, c, and e refer to the effect of screw speed, Figures 10.12b, d, and e portray the influence of output). Compounding in the TSE almost doubled the initial interlayer distance, but the influence of the operating conditions is complicated. Rheology and NIR indicate an increase of dispersion up to 100 rpm, followed by

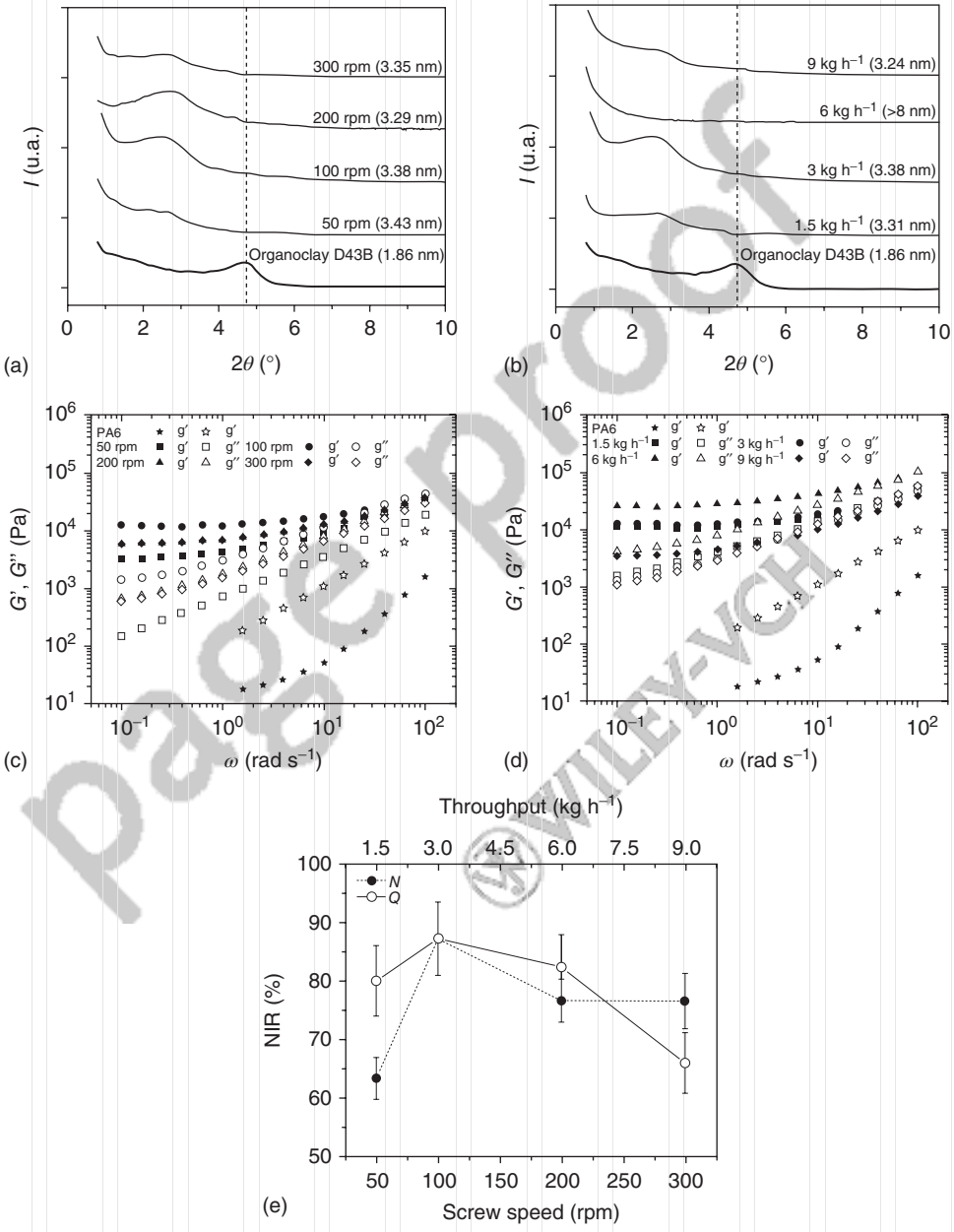

Figure 10.12 Effect of screw speed and output on final dispersion of a PA6/D43B nanocomposite: (a) effect of screw speed (XRD); (b) effect of output (XRD); (c) effect of screw speed (rheology); (d) effect of output (rheology); and (e) inline NIR. In the rheological curves PA6 denotes polymer matrix, whereas values of screw speed refer to the composites.

a decrease at upper speeds. This response is somewhat surprising, as increasing shear intensity resulting from higher screw speeds should stimulate intercalation [11]. As far as output is concerned, XRD data (Figure 10.12b) indicate an increase in intercalation with increasing throughput up to 6 kg h^{-1} (where the absence of the diffraction peak suggests a thoroughly exfoliated morphology), followed by a sharp drop when working at 9 kg h^{-1}. Identical trend is observed for the linear viscoelastic response (Figure 10.12d), with G' reaching the highest values for the composite produced at 6 kg h^{-1} and the lowest for 9 kg h^{-1}. NIR data (Figure 10.12e) also presents a maximum in dispersion at intermediate feed rates, even if it occurs at 3 kg h^{-1}.

It has been suggested that low feed rates promote intercalation because of the longer exposure of the material to hydrodynamic stresses [11]. However, this rise in residence time could stimulate the degradation of the clay surfactant and, eventually, of the polymer matrix. Such a phenomenon readily explains the lower rheological moduli. In turn, the corresponding lower melt viscosity would enable its draining out of the clay galleries, which could then eventually collapse and thus justify the lower interlayer distance estimated by XRD. Chemical degradation of the component(s) could also impact on the evolution of dispersion. Therefore, an optimum set of operating conditions maximizing final clay dispersion seems to exist.

10.7 Conclusions

In this chapter, the implementation of online and inline monitoring techniques capable of characterizing average clay dispersion levels during the preparation of polymer–clay nanocomposites by melt mixing was discussed. Using conventional compounding equipment, such as the Haake mixer and a corotating TSE, it was demonstrated that a method using NIR spectroscopy and suitable chemometrics was able to provide relevant real-time data, which was sensitive to changes in operating conditions, screw geometry, and material recipe. Also, the procedure could be readily implemented in industrial production scale. Measurements during mixing, or along the axis of the extruder, contributed to better understand the thermomechanical and chemical aspects involved in the dispersion of organoclays in polymeric matrices.

References

1. Auerbach, S.M. and Carrado, K.A. (2004) in *Handbook of Layered Materials* (ed. P.K. Dutta), Marcel Dekker, Inc., New York, Basel.
2. Alexandre, M. and Dubois, P. (2000) Polymer-layered silicate nanocomposites: preparation, properties and uses of a new class of materials. *Mater. Sci. Eng.*, **28**, 1–63.
3. Utracki, L.A. (2004) *Clay-Containing Polymer Nanocomposites*, vol. **1**, Rapra Technology Ltd.
4. Gupta, R.K., Kennel, E., and Kim, K. (2010) *Polymer Nanocomposites Handbook*, CRC Press.

Q10

5. Krishnamoorti, R., Vaia, R.A., and Giannelis, E.P. (1996) Structure and dynamics of polymer-layered silicate nanocomposites. *Chem. Mater.*, **8**, 1728–1734.
6. Giannelis, E.P. (1996) Polymer layered silicates nanocomposites. *Adv. Mater.*, **8**, 29–35.
7. Dennis, H.R., Hunter, D.L., Chang, D., Kim, S., White, J.L., Cho, J.W., and Paul, D.R. (2001) Effect of melt processing conditions on the extent of exfoliation in organoclay-based nanocomposites. *Polymer*, **42**, 9513–9522.
8. Solomon, M.J. and Somwangthanaroj, A. (2004) *Intercalated Polypropylene Nanocomposites*, Dekker Encyclopedia of Nanoscience and Nanotechnology, New York, pp. 1483–1490.
9. Krishnamoorti, R., Ren, J., and Silva, A.S. (2001) Shear response of layered silicate nanocomposites. *J. Chem. Phys.*, **114**, 4968–4973.
10. Koo, J.H. (2006) *Polymer Nanocomposites: Processing, Characterization and Applications*, McGraw-Hill.
11. Bousmina, M. (2006) Study of the intercalation and exfoliation processes in polymer nanocomposites. *Macromolecules*, **39**, 4259–4263.
12. Lertwimolnun, W. and Vergnes, B. (2006) Effect of processing conditions on the formation of polypropylene/organoclay nanocomposites in a twin-screw extruder. *Polym. Eng. Sci.*, **46**, 314–323.
13. Cho, J.W. and Paul, D.R. (2001) Nylon 6 nanocomposites by melt compounding. *Polymer*, **42**, 1083–1094.
14. Lertwimolnun, W. and Vergnes, B. (2007) Influence of screw profile and extrusion conditions on the microstructure of polypropylene/organoclay nanocomposites. *Polym. Eng. Sci.*, **47**, 2100–2109.
15. Pavlidou, S. and Papaspyrides, C.D. (2008) A review on polymer-layered silicate nanocomposites. *Prog. Polym. Sci.*, **33**, 1119–1198.
16. Ray, S.S. and Okamoto, M. (2003) Polymer/layered silicate nanocomposites: a review from preparation to processing. *Prog. Polym. Sci.*, **28**, 1539–1641.
17. Utracki, L.A. (2004) *Clay-Containing Polymer Nanocomposites*, vol. **2**, Rapra Technology Ltd.
18. Hussain, M., Hojjati, M., Okamoto, M., and Gorga, R.E. (2006) Polymer-matrix nanocomposites, processing, manufacturing and application: an overview. *J. Compos. Mater.*, **40**, 1511–1575.
19. Jang, B.N., Wang, D., and Wilkie, C.A. (2005) Relationship between the solubility parameter of polymers and the clay dispersion in polymer/clay nanocomposites and the role of the surfactant. *Macromolecules*, **38**, 6533–6543.
20. Paul, D.R. and Robeson, L.M. (2008) Polymer nanotechnology: nanocomposites. *Polymer*, **49**, 3187–3204.
21. Morgan, A.B. and Gilman, J.W. (2003) Characterization of polymer-layered nanocomposites by transmission electron microscopy and x-ray diffraction: a comparative study. *J. Appl. Polym. Sci.*, **87**, 1329–1338.
22. Bandyopadhyay, J. and Ray, S.S. (2010) The quantitative analysis of nano-clay dispersion in polymer nanocomposites by small angle X-ray scattering combined with electron microscopy. *Polymer*, **51**, 1437–1449.
23. Vermogen, A., Masenelli-Varlot, K., Séguéla, R., Duchet-Rumeau, J., Boucard, S., and Prele, P. (2005) Evaluation of the structure and dispersion in polymer-layered silicate nanocomposites. *Macromolecules*, **38**, 9661–9669.
24. Ren, J., Casanueva, B.F., Mitchell, C.A., and Krishnamoorti, R. (2003) Disorientation kinetics of aligned polymer layered silicate nanocomposites. *Macromolecules*, **36**, 4188–4194.
25. Wagener, R. and Reisinger, T. (2003) A rheological method to compare the degree of exfoliation of nanocomposites. *Polymer*, **44**, 7513–7518.
26. Durmus, A., Kasgoz, A., and Macosko, C.W. (2007) Linear low density polyethylene (LLDPE)/clay nanocomposites. Part I: structural characterization and quantifying clay dispersion by melt rheology. *Polymer*, **48**, 4492–4502.
27. Solomon, M.J., Almusallam, A.S., Seefeldt, K.F., Somwangthanaroj, A., and Varadan, P. (2001) Rheology of

polypropylene/clay hybrid materials. *Macromolecules*, **34**, 1864–1872.

28. Cassagnau, P. (2008) Melt-rheology of organoclay and fumed silica nanocomposites. *Polymer*, **49**, 2183–2196.
29. Lertwimolnun, W. and Vergnes, B. (2005) Influence of compatibilizer and processing conditions on the dispersion of nanoclay in a polymer matrix. *Polymer*, **46**, 3462–3471.
30. Vermant, J., Ceccia, S., Dolgovskij, M.K., Maffettone, P.L., and Macosko, C.W. (2007) Quantifying dispersion of layered nanocomposites via melt rheology. *J. Rheol.*, **51**, 429–450.
31. Xu, L., Nakajima, H., Manias, E., and Krishnamoorti, R. (2009) Tailored nanocomposites of polypropylene with layered silicates. *Macromolecules*, **42**, 3795–3803.
32. Tanoue, S., Utracki, L.A., Garcia-Rejon, A., Sammut, P., Ton-That, M.T., Pesneau, I., Kamal, M.R., and Lyngaae-Jorgensen, J. (2004) Melt compounding of different grades of polystyrene with organoclay. Part 2: rheological properties. *Polym. Eng. Sci.*, **44**, 1061–1076.
33. Ren, J. and Krishnamoorti, R. (2003) Nonlinear viscoelastic properties of layered-silicate-based intercalated nanocomposites. *Macromolecules*, **36**, 4443–4451.
34. Ren, J., Silva, A.S., and Krishnamoorti, R. (2000) Linear viscoelasticity of disordered polystyrene-polyisoprene block copolymer based layered-silicate nanocomposites. *Macromolecules*, **33**, 3739–3746.
35. VanderHart, D.L., Asano, A., and Gilman, J.W. (2001) NMR measurements related to clay-dispersion quality and organic modifier stability in nylon-6/clay nanocomposites. *Macromolecules*, **34**, 3819–3822.
36. VanderHart, D.L., Asano, A., and Gilman, J.W. (2001) Solid state NMR investigation of paramagnetic nylon-6 clay nanocomposites. 1. Crystallinity, morphology and the direct influence of Fe^{3+} on nuclear spins. *Chem. Mater.*, **13**, 3781–3795.
37. VanderHart, D.L., Asano, A., and Gilman, J.W. (2001) Solid state NMR investigation of paramagnetic nylon-6 clay nanocomposites. 2. Measurement of clay dispersion, crystal stratification and stability of organic modifiers. *Chem. Mater.*, **13**, 3796–3809.
38. Bourbigot, S., VanderHart, D.L., Gilman, J.W., Awad, W.H., Davis, R.D., Morgan, A.B., and Wilkie, C.A. (2003) Investigation of nanodispersion in polystyrene-montmorillonite nanocomposites by solid-state NMR. *J. Polym. Sci. B*, **41**, 3188–3213.
39. Loo, L.S. and Gleason, K.K. (2003) Fourier transform infrared investigation of the deformation behavior of montmorillonite in nylon-6/nanoclay nanocomposite. *Macromolecules*, **36**, 2587–2590.
40. Cole, K.C. (2008) Use of Infrared spectroscopy to characterize clay intercalation and exfoliation in polymer nanocomposites. *Macromolecules*, **41**, 834–843.
41. Cole, K.C., Perrin-Sarazin, F., and Dorval-Douville, G. (2005) Infrared spectroscopic characterization of polymer and clay platelet orientation in blown films based on polypropylene-clay nanocomposite. *Macromol. Symp.*, **230**, 1–10.
42. Ijdo, W.L., Kemnetz, S., and Benderly, D. (2006) An infrared method to assess organoclay delamination and orientation in organoclay polymer nanocomposites. *Polym. Eng. Sci.*, **46**, 1031–1039.
43. Johnston, C.T. and Premachandra, G.S. (2001) Polarized ATR-FTIR study of smectite in aqueous suspension. *Langmuir*, **17**, 3712–3718.
44. Bishop, J., Madejová, J., Komadel, P., and Fröschl, H. (2002) The influence of structural Fe, Al and Mg on the infrared OH bands in spectra of dioctahedral smectites. *Clay Miner.*, **37**, 607–616.
45. Hasegawa, N., Okamoto, H., Kato, M., and Usuki, A. (2000) Preparation and mechanical properties of polypropylene-clay hybrids based on modified polypropylene and organophilic clay. *J. Appl. Polym. Sci.*, **78**, 1918–1922.

46. Miltner, H.E., Watzeels, N., Block, C., Gotzen, N.A., Van Assche, G., Borghs, K., Van Durme, K., Van Mele, B., Bogdanov, B., and Rahier, H. (2010) Qualitative assessment of nanofiller dispersion in poly(ϵ-caprolactone) nanocomposites by mechanical testing, dynamic rheometry and advanced thermal analysis. *Eur. Polym. J.*, **46**, 984–996.

47. Vaia, R.A., Ishii, H., and Giannelis, E.P. (1993) Synthesis and properties of two-dimensional nanostructures by direct intercalation of polymer melts in layered-silicates. *Chem. Mater.*, **5**, 1694–1696.

48. Fornes, T.D., Yoon, P.J., Keskkula, H., and Paul, D.R. (2001) Nylon 6 nanocomposites: the effect of matrix molecular weight. *Polymer*, **42**, 9929–9940.

49. Kim, S.W., Jo, W.H., Lee, M.S., Ko, M.B., and Jho, J.Y. (2002) Effects of shear on melt exfoliation of clay in preparation of nylon 6/organoclay nanocomposites. *Polym. J.*, **34**, 103–111.

50. Tanoue, S., Utracki, L.A., Garcia-Rejon, A., Ttibouet, J., Cole, K.C., and Kamal, M.R. (2004) Melt compounding of different grades of polystyrene with organoclay. Part 1: compounding and characterization. *Polym. Eng. Sci.*, **44**, 1046–1060.

51. Xanthos, M. (ed.) (1992) *Reactive Extrusion*, Hanser Publishers, New York.

52. Galgali, G., Ramesh, C., and Lele, A. (2001) A rheological study on the kinetics of hybrid formation in polypropylene nanocomposites. *Macromolecules*, **34**, 852–858.

53. Chrissopoulou, K. and Anastasiadis, S.H. (2011) Polyolefin/layered silicate nanocomposites with functional compatibilizers. *Eur. Polym. J.*, **47**, 600–613.

54. Treece, M.A., Zhang, W., Moffit, R.D., and Oberhauser, J.P. (2007) Twin-screw extrusion of polypropylene-clay nanocomposites: Influence of masterbatch processing, screw rotation mode and sequence. *Polym. Eng. Sci.*, **47**, 898–911.

55. Médéric, P., Ville, J., Huitric, J., Moan, M., and Aubry, T. (2011) Effect of processing procedures and conditions on structural, morphological and rheological properties of polyethylene/polyamide/nanoclay blends. *Polym. Eng. Sci.*, **51**, 969–978.

56. Dynisco Online Rheometer (Viscosensor), *http://www.dynisco.com* (accessed 23 April 2014).

57. Zschuppe, V., Geilen, T., Maia, J.M., Covas, J.A., and Petri, H.M. (2006) Rheology Application Note LR-57: Thermo Electron Corporation.

58. Hsiao, B.H., Barton, R. Jr., and Quintana, J. (1996) Simple on-line x-ray setup to monitor structure changes during fiber processing. *J. Appl. Polym. Sci.*, **62**, 2061–2068.

59. Chu, B. and Hsiao, B.S. (2001) Small-angle x-ray scattering of polymers. *Chem. Rev.*, **101**, 1727–1761.

60. Heeley, E.L., Gough, T., Bras, W., Gleeson, A.J., Coates, P.D., and Ryan, A.J. (2005) Polymer processing: using synchrotron radiation to follow structure development in commercial and novel polymer materials. *Nucl. Instrum. Methods Phys. Res. B*, **238**, 21–27.

61. Kolb, R., Seifert, S., Stribeck, N., and Zachman, H.G. (2000) Simultaneous measurements of small- and wide-angle X-ray scattering during low speed spinning of polypropylene using synchrotron radiation. *Polymer*, **41**, 1497–1505.

62. Nogales, A., Hsiao, B.S., Somani, R.H., Srinivas, S., Tsou, A.H., Balta-Calleja, F.J., and Ezquerra, T.A. (2001) Shear induced crystallization of isotactic polypropylene with different molecular weight distributions: in-situ small- and wide-angle X-ray scattering studies. *Polymer*, **42**, 5247–5256.

63. Ran, S., Burger, C., Sics, I., Yoon, K., Fang, D., Kim, K., Avila-Orta, C., Keum, J., Chu, B., Hsiao, B.S., Cookson, D., Shultz, D., Lee, M., Viccaro, J., and Ohta, Y. (2004) In situ synchrotron SAXS/WAXD studies during melt spin of modified carbon nanofiber and isotactic polypropylene nanocomposite. *Colloid Polym. Sci.*, **282**, 802–809.

64. Yamaguchi, T., Komoriyama, K., Ohkoshi, Y., Urakawa, H., Gotoh, Y., Terasawa, N., Nagura, M., and Kajiwara, K. (2005) Online wide-angle X-ray diffraction/small-angle x-ray scattering measurements for the CO_2-laser-heated drawing of poly(ethylene terephthalate) fiber. *J. Polym. Sci. B*, **43**, 1090–1099.
65. Ellison, M.S., Lopes, P.E., and Pennington, W.T. (2008) In-situ x-ray characterization of fiber structure during melt spinning. *J. Eng. Fibers Fabr.*, **3**, 10–21.
66. Dealy, M., Broadhead, T.O., and Collyer, A.A. (eds) (1993) *Techniques in Rheological Measurement*, Chapman & Hall, London.
67. Covas, J.A., Nóbrega, J.M., and Maia, J.M. (2000) Rheological measurements along an extruder with an on-line capillary rheometer. *Polym. Test.*, **19**, 165–176.
68. Dogan, N., McCarthy, M.J., and Powell, R.L. (2005) Measurements of polymer melt rheology using ultrasonic-based in-line rheometry. *Meas. Sci. Technol.*, **16**, 1684–1690.
69. Wiklund, J., Shahram, I., and Stading, M. (2007) Methodology for in-line rheology by ultrasound Doppler velocity profiling and pressure difference techniques. *Chem. Eng. Sci.*, **62**, 4277–4293.
70. Smith, R.S. and Glasscock, J.A. (2004) Measurements of the rheological properties of standard reference material 2490 using an in-line micro-Fourier rheometer. *Korea-Aust. Rheol. J.*, **16**, 169–173.
71. Baird, D.G., Chan, T.W., McGrady, C., and Mazahir, S.M. (2010) Evaluation of the use of a semi-hyperbolic die for measuring elongational viscosity of polymer melts. *Appl. Rheol.*, **20**, 34900–34912.
72. Covas, J.A., Maia, J.M., Machado, A.V., and Costa, P. (2008) On-line rotational rheometry for extrusion and compounding operations. *J. Non-Newtonian Fluid Mech.*, **148**, 88–96.
73. Thermo SCIENTIFIC (2006) HAAKE ProFlow, *http://www.thermo.com/eThermo/CMA/PDFs/Product/ProductPDF_18544.pdf.* (accessed 23 April 2014).
74. Goettfert Göttfert Process Rheometers, *http://www.goettfert.com* (accessed 23 April 2014).
75. Kaylon, D.M. and Gokturk, H.S. (1994) Adjustable gap rheometer. US Patent No 5, 277, 058, Hoboken, NJ.
76. Mould, S., Barbas, J.M., Machado, A.V., Nóbrega, J.M., and Covas, J.A. (2011) Measuring the rheological properties of polymer melts with on-line rotational rheometry. *Polym. Test.*, **30**, 602–610.
77. Alig, I., Steinhoff, B., and Lellinger, D. (2010) Monitoring of polymer melt processing. *Meas. Sci. Technol.*, **21**, 1–19.
78. Fischer, D., Müller, J., Kummer, S., and Kretzschmar, B. (2011) Real time monitoring of morphologic and mechanical properties of polymer nanocomposites during extrusion by near infrared and ultrasonic spectroscopy. *Macromol. Symp.*, **35**, 10–17.
79. George, G., Hynard, N., Cash, G., Rintoul, L., and O'Shea, M. (2006) Spectroscopic probes for real-time monitoring of polymer modification and degradation reactions. *C.R. Chim.*, **9**, 1433–1443.
80. Coates, P.D., Barnes, S.E., Sibley, M.G., Brown, E.C., Edwards, H.G., and Scowen, I.J. (2003) In-process vibrational spectroscopy and ultrasound measurements in polymer melt extrusion. *Polymer*, **44**, 5937–5949.
81. Alig, D.F., Lellinger, D., and Steinhoff, B. (2005) Combination of NIR, Raman, Ultrasonic and Dielectric spectroscopy for in-line monitoring of the extrusion process. *Macromol. Symp.*, **230**, 51–58.
82. Barnes, S.E., Sibley, M.G., Edwards, H.G., and Coates, P.D. (2007) Process monitoring of polymer melts using in-line spectroscopy. *Trans. Inst. Meas. Control*, **29**, 453–465.
83. Wang, Y., Steinhoff, B., Brinkmann, C., and Alig, I. (2008) In-line monitoring of the thermal degradation of poly (L-lactic acid) during melt extrusion by UV-vis spectroscopy. *Polymer*, **49**, 1257–1265.
84. Fischer, D., Sahre, K., Abdelrhim, M., Voit, B., Sahdu, V.B., Pionteck, J.,

Komber, H., and Hutschenreuter, J. (2006) Process monitoring of polymers by ATR-IR, NIR and Raman spectroscopy and ultrasonic measurements. *C. R. Chim.*, **9**, 1419–1424.

85. Villanueva, M.P., Cabedo, L., Giménez, E., Lagarón, J.M., Coates, P.D., and Kelly, A.L. (2009) Study of the dispersion of nanoclays in a LDPE matrix using microscopy and in-process ultrasonic monitoring. *Polym. Test.*, **28**, 277–287.

86. Lee, Y.-H., Bur, A.J., Roth, S.C., Start, P.R., and Harris, R.H. (2005) Monitoring the relaxation behavior of nylon/clay nanocomposites in the melt with an online dielectric sensor. *Polym. Adv. Technol.*, **16**, 249–256.

87. Bur, A.J., Lee, Y.-H., Roth, S.C., and Start, P.R. (2005) Measuring the extent of exfoliation in polymer/clay nanocomposites using real-time process monitoring methods. *Polymer*, **46**, 10908–10918.

88. Rodd, T.R. (2002) Fiber-optic probes for near-infrared spectrometry. [autor do livro], in *Handbook of Vibration Spectroscopy*, Sampling Techniques, vol. **2** (eds P.R. Griffiths and J.M. Chalmers), John Willey & Sons, Ltd, Chichester.

89. Tate, J.D., Chauvel, P., Guenard, R.D., and Harner, R. (2002) Process monitoring by mid- and near-infrared Fourier transform spectroscopy. [autor do livro], in *Handbook of Vibration Spectroscopy*, Applications in Industry, Materials and the Physical Sciences, vol. **4** (eds P.R. Griffiths and J.M. Chalmers), John Willey & Sons, Ltd, Chichester.

90. Rohe, T., Becker, W., Kölle, S., Eisenreich, N., and Eyerer, P. (1999) Near infrared (NIR) spectroscopy for in-line monitoring of polymer extrusion processes. *Talanta*, **50**, 283–290.

91. Nagata, T., Oshima, M., and Tanigaki, M. (2000) In-line monitoring of polyethylene density using near infrared (NIR) spectroscopy. *Polym. Eng. Sci.*, **40**, 1107–1113.

92. Barrès, C., Bounor-Legaré, V., Melis, F., and Michel, A. (2006) In-line near infrared monitoring of esterification of a molten ethylene–vinyl alcohol copolymer in a twin screw extruder. *Polym. Eng. Sci.*, **46**, 1613–1624.

93. Ghita, O.R., Baker, D.C., and Evans, K.E. (2008) An in-line near-infrared process control tool for monitoring the effects of speed, temperature, and polymer color in injection molding. *Polym. Test.*, **27**, 459–469.

94. Cherfi, A., Fevotte, G., and Novat, C. (2002) Robust on-line measurement of conversion and molecular weight using NIR spectroscopy during solution polymerization. *J. Appl. Polym. Sci.*, **85**, 2510–2520.

95. Othman, N.S., Fevotte, G., Peycelon, D., Egraz, J.-B., and Suau, J.-M. (2004) Control of polymer molecular weight using near infrared spectroscopy. *AIChE J.*, **50**, 654–664.

96. Reis, M.M., Araújo, P.H., Sayer, C., and Giudici, R. (2007) Spectroscopic on-line monitoring of reactions in dispersed medium: chemometric challenges. *Anal. Chim. Acta*, **595**, 257–265.

97. Rodriguez-Guadarrama, L.A. (2007) Application of online near infrared spectroscopy to study the kinetics of anionic polymerization of butadiene. *Eur. Polym. J.*, **43**, 928–937.

98. Moghaddam, L., Martin, D.J., Halley, P.J., and Fredericks, P.M. (2009) Vibrational spectroscopic studies of laboratory scale polymer melt processing: application to a thermoplastic polyurethane nanocomposite. *Vib. Spectrosc.*, **51**, 86–92.

99. Lachenal, G. (1997) Characterization of poly(ethylene terephthalate) using near and far FTIR spectroscopy. *Int. J. Polym. Anal. Character.*, **3**, 145–158.

100. Heikka, R.A., Immonen, K.T., Minkkinen, P.O., Paatero, E.Y.O., and Salmi, T.O. (1997) Determination of acid value, hydroxyl value and water content in reactions between dicarboxylic acids and diols using near-infrared spectroscopy and non-linear partial least squares regression. *Anal. Chim. Acta*, **349**, 287–294.

101. Amari, T. and Ozaki, Y. (2002) Generalized two-dimensional attenuated total reflection/infrared and near-infrared correlation spectroscopy studies of

real-time monitoring of the initial oligomerization of bis(hydroxyethyl terephthalate). *Macromolecules*, **35**, 8020–828.

102. Tuchbreiter, A., Kappler, B., Stockmann, R., Mülhaupt, R., and Honerkamp, J. (2003) Near-infrared reflection spectroscopy: a versatile tool for rapid characterization of olefin copolymers and high throughput experiments. *Macromol. Mater. Eng.*, **288**, 29–34.

103. Marengo, E., Bobba, M., Robotti, E., and Lenti, M. (2004) Hydroxyl and acid number prediction in polyester resins by near infrared spectroscopy and artificial neural networks. *Anal. Chim. Acta*, **511**, 313–322.

104. Blanco, M., Cruz, J., and Armengol, M. (2008) Control production of polyester resins by NIR spectroscopy. *Microchem. J.*, **90**, 118–123.

105. Santos, A.F., Lima, E.L., and Pinto, J.C. (1998) In-line evaluation of average particle size in styrene suspension polymerizations using Near-Infrared spectroscopy. *J. Appl. Polym. Sci.*, **70**, 1737–1745.

106. Santos, A.F., Lima, E.L., and Pinto, J.C. (2000) Control and design of average particle size in styrene suspension polymerizations using NIRS. *J. Appl. Polym. Sci.*, **77**, 453–462.

107. Zhou, Q., Xi, Y., He, H., and Frost, R.L. (2008) Application of near infrared spectroscopy for the determination of adsorbed p-nitrophenol on HDTMA organoclay—implications for the removal of organic pollutants from water. *Spectrochim. Acta Part A*, **69**, 835–841.

108. Madejová, J., Pentrák, M., Pállková, H., and Komadel, P. (2009) Near-infrared spectroscopy: a powerful tool in studies of acid-treated clay minerals. *Vib. Spectrosc.*, **49**, 211–218.

109. Frost, R.L., Spratt, H.J., and Palmer, S.J. (2009) Infrared and near-infrared spectroscopic study of synthetic hydrotalcites with variable divalent/trivalent cationic ratios. *Spectrochim. Acta Part A.*, **72**, 984–988.

110. Lui, R., Frost, R.L., and Martens, W.N. (2009) Near infrared and mid infrared investigations of adsorbed phenol on HDTMAB organoclays. *Mater. Chem. Phys.*, **113**, 707–713.

111. Madejová, J., Pálková, H., and Komadel, P. (2006) Behaviour of Li+ and Cu2+ in heated montmorillonite: evidence from far-, mid-, and near-IR regions. *Vib. Spectrosc.*, **40**, 80–88.

112. Frost, R.L., Kloprogge, J.T., and Ding, Z. (2002) Near-infrared spectroscopic study of nontronites and ferruginous smectite. *Spectrochim. Acta Part A*, **58**, 1657–1668.

113. Laske, S., Kracalik, M., Feuchter, M., Pinter, G., Maier, G., Märzinger, W., Haberkorn, M., and Langecker, G.R. (2009) FT–NIR as a determination method for reinforcement of polymer nanocomposites. *J. Appl. Polym. Sci.*, **114**, 2488–2496.

114. Witschnigg, A., Laske, S., Kracalik, M., Feuchter, M., Pinter, G., Maier, G., Märzinger, W., Haberkorn, M., Langecker, G.R., and Holzer, C. (2010) In-Line characterization of polypropylene nanocomposites using FT-NIR. *J. Appl. Polym. Sci.*, **117**, 3047–3053.

115. Blanco, M. and Villarroya, I. (2002) NIR spectroscopy: a rapid-response analytical tool. *Trends Anal. Chem.*, **21**, 240–249.

116. Burns, D.A. and Ciurczak, E.W. (eds) (2008) *Handbook of Near-Infrared Analysis*, CRC Press.

117. Siesler, H.W., Ozaki, Y., Kawata, S., and Heise, H.M. (eds) (2002) *Near-Infrared Spectroscopy: Principles, Instruments, Applications*, Wiley-VCH Verlag GmbH, Weinheim.

118. Workman, J. Jr., and Weyer, L. (2007) *Practical Guide to Interpretive Near-Infrared Spectroscopy*, CRC Press, Boca Raton, FL.

119. Adams, M.J. (1995) *Chemometrics in Analytical Spectroscopy*, The Royal Society of Chemistry.

120. Barbas, J.M., Machado, A.V., and Covas, J.A. (2012) In-line near-infrared spectroscopy for the characterization of dispersion in polymer-clay nanocomposites. *Polymer Test.*, **31**, 527–536.

121. Covas, J.A., Carneiro, O.S., Maia, J.M., Filipe, S.A., and Machado, A.V. (2002)

Evolution of chemistry, morphology and rheology of various polymer systems along a twin-screw extruder. *Can. J. Chem. Eng.*, **80**, 1065–1074.

122. Lee, J.K. and Han, C.D. (1999) Evolution of polymer blend morphology during compounding in an internal mixer. *Polymer*, **40**, 6277–6296.

123. Kim, D.H., Fasulo, P.D., Rodgers, W.R., and Paul, D.R. (2007) Structure and properties of polypropylene-based nanocomposites: effect of PP-g-MA to organoclay ratio. *Polymer*, **48**, 5308–5323.

124. Barbas, J.M., Machado, A.V., and Covas, J.A. (2013) In-line near-infrared spectroscopy: a tool to monitor the preparation of polymer-clay nanocomposites in extruders. *J. Appl. Polym. Sci.*, **127**, 4899–4909.

125. Barbas, J.M., Machado, A.V., and Covas, J.A. (2013) Evolution of dispersion along the extruder during the manufacture of polymer–organoclay nanocomposites. *Chem. Eng. Sci.*, **98**, 77–87.

126. Barbas, J.M., Machado, A.V., and Covas, J.A. (0000) Effect of processing conditions on development of dispersion is a twin screw extruder: polypropylene-clay nanocomposites. *Chem. Eng. Technol.*, in press.

127. Barbas, J.M., Machado, A.V., and Covas, J.A. (0000) Evolution of dispersion of polyamide 6-clay nanocomposites along the extruder: effect of processing conditions. *Macromolecules*, Submitted.♦ Q11

"keywords/abstract

Dear Author,

Keywords and abstracts will normally not be included in the print version of your chapter but only in the online version (if not decided differently by Wiley-VCH).

Thank you!"

Abstract

Keywords

Affiliation for the Authors: Ana Vera Machado, J.M. Barbas, and J.A. Covas
Institute of Polymers and Composites (IPC) and I3N, University of Minho, Guimarães, Portugal

Queries in Chapter 10

Q1. Please spell out the forename for the authors Barbas and Covas.

Q2. Please provide department name and street name for the affiliation of the authors Machado, Barbas and Covas.

Q3. Please provide permission details for Figures 10.1 to 10.6.

Q4. As references 78 and 115 are identical, 115 has been replaced with 78 and subsequent references have been renumbered to maintain sequence in the text.

Q5. Please confirm if the abbreviation of 'TPU' should be 'polyurethane' or 'Thermoplastic polyurethane'.

Q6. Please confirm if the expansion "Polypropylene/Polypropylene grafted with Maleic Anhydride/Montmorillonite/Cloisite 20A system" provided for "PP/PP-g-MA/C20A" is OK here.

Q7. As references 29 and 124 are identical, 124 has been replaced with 29 and subsequent references have been renumbered to maintain sequence in the text.

Q8. As references 53 and 126 are identical, 126 has been replaced with 53 and subsequent references have been renumbered to maintain sequence in the text.

Q9. Please confirm if the expansion of 'Polypropylene/Polypropylene grafted with Maleic Anhydride/Organo-Montmorillonite' should be 'PP/PP-g-MA/D67G' or 'PP/PP-g-MA/OMMT'.

Q10. Please note that references have been renumbered to maintain sequential order of text citations.

Q11. Please clarify if this article has since been published. If so, please provide the volume number and page range for References 126, 127.